Available online at www.sciencedirect.com
ScienceDirect
International Journal of Heat and Mass Transfer 50 (2007) 4540–4553
International Journal of HEAT and MASS TRANSFER
www.elsevier.com/locate/ijhmt

Oscillatory double-diffusive mixed convection in a two-dimensional ventilated enclosure

Brahim Ben Beya *, Taieb Lili

Laboratoire de Mécanique des Fluides, Faculté des Sciences de Tunis, Dpt de Physique, 2092 El Manar 2 Tunis, Tunisia

Received 11 May 2006; received in revised form 10 March 2007
Available online 23 May 2007

Abstract

By starting from a steady flow configuration based on the work of Deng et al. [Qi-Hong Deng, Jiemin Zhou, Chi Mei, Yong-Ming Shen, Fluid, heat and contaminant transport structures of laminar double-diffusive mixed convection in a two-dimensional ventilated enclosure, Int. J. Heat Mass Transfer 47 (2004) 5257–5269], a numerical investigation was conducted to analyse the unsteady double-diffusive mixed convection in two-dimensional ventilated room due to heat and contaminant sources. Owing to the large number of parameters, the results are reported only for a constant buoyancy ratio N equal to 1. The flow is found to be oscillatory for a fixed Reynolds number ($700 \leqslant Re \leqslant 1000$) when the Grashof number is varied in a wide range ($10^3 \leqslant Gr \leqslant 10^6$). Results of the simulations show that the onset of the oscillatory indoor airflow occurs for couples (Re, Gr) values that can be correlated as $Re = aGr^b$.

Keywords: Unsteady flow; Double diffusion; Mixed convection; Contaminant source; Multigrid method

1. Introduction

Double-diffusive mixed convection is caused by the temperature and concentration gradients in the fluid, in which the heat and mass transfer occur simultaneously, and some external applied forces. Double-diffusive convection in stationary heat and mass transfer problems in enclosures has received attention mostly over the past decade [2–6].

Recently, considerable attention has turned to mixed combined (heat and mass) convection in open cavities flow problems because of a number of practical applications. For example, these include electronic cooling, pollution, thermal insulations, drying chamber, and thermal environmental control of buildings etc.

People in developed societies spend the majority of their time indoors; indoor air environment has changed enormously to improve health, comfort, and productivity [7]. Obviously, a poor indoor air quality condition, such as uncomfortable micro-climate, smoking, cooking, etc is dangerous for health. Indoor environments of rooms are needed to be more thermally comfortable and healthy as the residence time indoors has gradually increased. Furthermore, there have been some studies dealing with ventilated enclosure problems with one or two sources. Earlier, Chung [8], investigated the air movement and contaminant transport in a partitioned enclosure with ventilation. The standard two-equation turbulent model was used. The computed results of temperature and velocity fields agreed well with the measured data. Deng and Tang [9] presented a two-dimensional, steady, laminar model to analyse interaction between natural and forced convection. In their study, the authors show that the use of the ventilation system improves indoor air quality. Subsequently, a numerical study on the double-diffusive mixed convection in a two-dimensional ventilated enclosure due to discrete heat and contaminant sources were carried out by Deng et al. [1] and Deng and Zhang [10]. This related topic of their studies deals with the double-diffusive mixed convection which plays a dominant role to predict the indoor air environment.

* Corresponding author. Fax: +216 71871666.
E-mail address: Brahim.benbeya@fst.rnu.tn (B.B. Beya).

0017-9310/$ - see front matter © 2007 Elsevier Ltd. All rights reserved.
doi:10.1016/j.ijheatmasstransfer.2007.03.027

Nomenclature

a	length of heat/contaminant source (m)
C	concentration (kg m^{-3})
D	mass diffusivity (m^2 s^{-1})
f	frequency (Hz)
g	gravity acceleration (m s^{-2})
Gr	Grashof number, $Gr = g\beta_T \Delta T \cdot H^3/\nu^2$
h	sizes of inlet and outlet (m)
H	enclosure height (m)
L	length of enclosure (m)
Le	Lewis number, $Le = \alpha/D$
N	Buoyancy ratio number, $N = \beta_C \Delta C/\beta_T \Delta T$
n	unit vector normal to the control volume surface
Nu	average Nusselt number, defined in Eq. (5)
P	pressure (Pa)
p	dimensionless pressure, $p = P/\rho U_i^2$
Pr	Prandtl number, $Pr = \nu/\alpha$
Re	Reynolds number, $Re = U_i H/\nu$
Sc	Schmidt number, $Sc = \nu/D$
Sh	average Sherwood number defined in Eq. (6)
T	temperature (K)
t	dimensionless time, $t = H/U_i$
U, V	velocity components (ms^{-1})
u, v	dimensionless velocity components, in x and y directions $(u, v) = (U, V)/U_i$
X, Y	cartesian coordinates (m)
x, y	dimensionless Cartesian coordinates, $(x, y) = (X, Y)/H$

Greek symbols

α	thermal diffusivity (m^2 s^{-1})
β_T	coefficient of thermal expansion (K^{-1})
β_C	coefficient of solutal expansion (Kg^{-1} m^3)
ν	kinematics viscosity (m^2 s^{-1})
ρ	density of air (kg m^{-3})
τ	dimensionless period
θ	dimensionless temperature , $\theta = (T - T_i)/\Delta T$
Δt	dimensionless time step
ΔT	temperature scale, $\Delta T = T_h - T_i$
Δc	concentration scale, $\Delta C = C_h - C_i$
ψ	dimensionless stream-function
H	dimensionless heat-function
M	dimensionless mass-function

Subscripts

i	inlet
h	high
n	time level
C	concentration
T	temperature

The main goal of the study reported by Deng et al. [1] is to characterise the airflow and heat/contaminant transport structures in indoor air environment. Their results clearly underscore the effectiveness of using a numerical visualization in terms of streamlines, heatlines, and masslines. Attention is given to analyse the two kinds of convection involved in the ventilated room through the effects of the main factors, namely Grashof number (Gr), Reynolds number (Re), buoyancy ratio (N); as well as the ventilation mode. The value of Re was varied in the range of 100–700 and for a fixed Re value, those for Gr were varied ($10^3 \leqslant Gr \leqslant 2.510^5$) until a stable solution could not be obtained. The analysis was also focused on a range of solutal to thermal buoyancy ratios ($0.1 \leqslant N \leqslant 10$).

The authors reported that the airflow structure is determined by the relation between the natural and forced convection. Their maximum competition is correlated as $Re = 0.0125Gr + 272.41$ at ($10^3 \leqslant Gr \leqslant 3.10^4$) and ($300 < Re < 700$). In addition, their results show that the contaminant removal efficiencies depend on the importance of two convection mechanisms.

All the works cited above deal with stationary flows implying no appearance of the time derivative in the governing equations and questions related with unsteady solutions are intentionally avoided.

Recent developments in engineering have led to an increasing interest in transient mixed convection flows. These flows arise in many technological applications such as nuclear plants, heat exchangers and other apparatus, etc. The spontaneous appearance of unsteady regimes can be observed for certain values of combinations of governing parameters, or when the boundary conditions are normally changing in time. In general, thermal transfer and mixing depend largely on unsteady state, and so the formulation for studying such systems must take into account the transient phenomena.

A number of studies have been focused on transient double-diffusive problems [11–13]. Nishimura et al. [14] investigated the oscillatory double-diffusive convection in a rectangular enclosure with combined horizontal temperature and concentration gradients. It was found that the oscillatory regime occurs for a certain range of buoyancy ratio. The onset of double-diffusive convection in a rectangular porous cavity with mixed boundary conditions for heat and solute has been studied numerically by Mahidjiba et al. [15] using linear stability analysis. The onset of convection was found to be dependent of the most of the problem parameters. Subsequently, a high order difference scheme was proposed by Zhan and Li [16], for resolving the oscillatory flow phenomenon in double-diffusive prob-

lem under the boundary fitted coordinate system. The authors found that when the Lewis number (Le) is great than unity multiple eddies appear during the cycle of oscillations, elsewhere the steady motion becomes progressively more unsteady as the value of the Lewis number decreases. Recently, Shi and Lu [17] studied numerically the time evolution of double-diffusive convection in a vertical cylinder with radial temperature and axial solutal gradients using a finite element method. It was shown that the average Nusselt number (Nu) at the sidewall remains almost unchanged while the average Sherwood number (Sh) at the bottom wall changes much for some values of the buoyancy ratio N.

The previous work which is closely relevant to the present investigation appears to be the numerical study reported by Deng et al. [1] presented above. As was pointed earlier, their results cover only the steady airflow regime (stationary form of the governing equations where is no time evolution in the fields).

To the best knowledge of the author, no attention has been paid to the transient double-diffusive mixed convection in the ventilated room. In the present study, we extend the work of Deng et al. [1] which concerns the double-diffusive mixed convection in a two-dimensional ventilated enclosure due to the discrete heat and contaminant sources, to the unsteady case. We would like to point out the limitations calculus made with the assumption of stationary flows by reaching the main following objectives:

(i) predict numerically what ranges in governing parameter values are necessary to make airflow in ventilated room oscillatory,
(ii) describe the transition to the periodic airflow according to the pertinent parameters under study,
(iii) show that there are differences in some physical phenomena which occur in the unsteady airflow case by comparison with the steady results,
(iv) prove changes in heat and mass transfer characteristics including the unsteady airflow regime, steady laws will not be valuable.

Analysis of questions related to the stability flow or bifurcation is not the focus of our study. Probably further studies with large ranges of governing parameters are necessary to clarify this matter.

2. Mathematical model

2.1. Problem definition

The problem is a two-dimensional double-diffusive mixed convection. This problem with the same geometry and boundary conditions was considered by Deng et al. [1] where steady computed was applied. The problem geometry and boundary conditions are shown in Fig. 1. It is a two-dimensional ventilated room of height H and width L (aspect ratio L/H), with two opening. The two

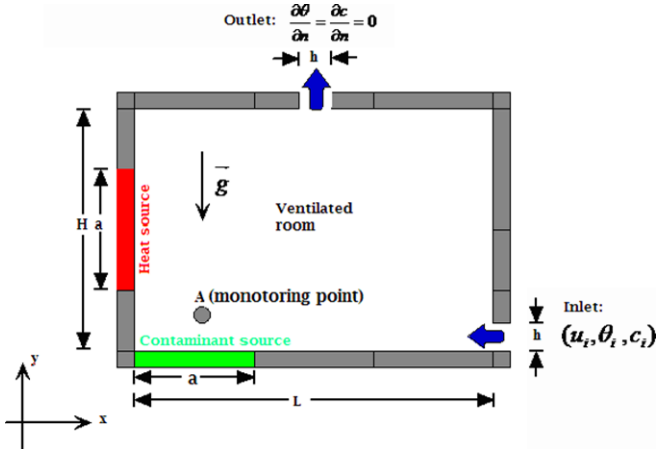

Fig. 1. Schematic of 2-D double-diffusive mixed convection in a ventilated room. A is the monitoring point with dimensionless coordinates $(x, y) = (0.25, 0.125)$.

opening are placed at bottom and top, to allow the admission of outside fresh air and the passage of the heated air outside the room, respectively. The inlet and outlet are the same size, h. A heat source of size a and high temperature T_h, locates center on the left wall, and a contaminant source of equal size and high concentration C_h on the left part of the floor. The forced flow of fresh air, imposed at the bottom of right sidewall of the lower opening, has a temperature T_i, a concentration C_i and a horizontal velocity U_i ($T_i < T_h$, $C_i < C_h$). Other parts of the enclosure are all considered adiabatic and impermeable. Moreover, the cavity is supposed to be sufficiently deep in the third direction so that the hypothesis of two-dimensional study is valid according to the stationary flow. This hypothesis may be changed if the flow becomes unsteady.

2.2. Governing equations

The double-diffusive mixed convection is assumed to be two-dimensional, unsteady and laminar. The fluid is Newtonian and incompressible. Also, all thermophysical properties of the fluid are taken to be constant except for the density variation in the buoyancy term, where the Boussinesq approximation is considered as: $\rho = \rho_0[1 - \beta_T(T - T_0) - \beta_C(C - C_0)]$, ($\rho_0$, T_0, C_0 are the reference density, temperature and concentration), where β_T and β_C are the coefficients for thermal and concentration expansions, respectively such that

$$\beta_T = -\frac{1}{\rho_0}\left(\frac{\partial\rho}{\partial T}\right)_{P,C} \quad \text{and} \quad \beta_C = -\frac{1}{\rho_0}\left(\frac{\partial\rho}{\partial C}\right)_{P,T}.$$

The governing equations are non-dimensionalized using H, the height of the cavity, as the scale factor length; U_i, H/U_i and ρU_i^2 as the scaling factor for velocity, time and pressure, respectively. $\Delta T = T_h - T_i$ and $\Delta C = C_h - C_i$ are the characteristic scales for temperature and concentration, respectively. Dimensionless variables are introduced as

follows to cast the governing equations in dimensionless forms:

$$(x, y) = (X, Y)/H, \quad (u, v) = (U, V)/U_i, \quad p = P/\rho U_i^2,$$
$$\theta = (T - T_i)/\Delta T, \quad c = (C - C_i)/\Delta C.$$

The dimensionless form of the governing equations, which describe the fluid motion, energy and concentration transports in the enclosure, written in Cartesian coordinates, are given by:

$$\nabla \cdot \vec{u} = 0, \tag{1}$$

$$\frac{\partial \vec{u}}{\partial t} + (\vec{u} \cdot \nabla)\vec{u} = -\nabla p + \frac{1}{Re}\nabla^2 \vec{u} + \frac{Gr}{Re^2}(\theta + Nc)\vec{e_y}, \tag{2}$$

$$\frac{\partial \theta}{\partial t} + \nabla \cdot (\theta \vec{u}) = \frac{1}{PrRe}\nabla^2 \theta \tag{3}$$

$$\frac{\partial c}{\partial t} + \nabla.(c\vec{u}) = \frac{1}{ScRe}\nabla^2 c, \tag{4}$$

where $\vec{u}$ the dimensionless velocity and p is is the dimensionless acting pressure. Foregoing equations introduce the following dimensionless numbers:

The Reynolds number, Re, which characterise the forced convection, Gr is related to the natural convection and N is the buoyancy ratio number which is the ratio between the solute and thermal buoyancy forces. It can be either positive or negative. When N is a positive, the temperature and concentration buoyancy effects are combined, and they are opposite otherwise. However, in the present study, the polluted gas indoors is assumed lighter then air.

For the initial conditions, the fluid temperature and concentration in the entire domain has the same temperature and concentration as the corresponding reference values at the cold wall ($\theta = c = 0$).

2.2.1. Boundary conditions

The boundary conditions are shortly summarized as:

At inlet: $u = -1$ and $v = 0$, $\theta = 0$, $c = 0$;
At outlet: $u = 0$ and $v = 1$, $\partial\theta/\partial\mathbf{n} = 0$, $\partial c/\partial\mathbf{n} = 0$;
Walls: $u = v = 0$, $\theta = 1$ for the heat source and $\partial\theta/\partial\mathbf{n} = 0$ elsewhere, $c = 1$ for the contaminant source and $\partial c/\partial\mathbf{n} = 0$ elsewhere.

2.3. Fluid, heat and mass transfer parameters

The heat and mass transfer rates on the surfaces of heat and contaminant sources can be evaluated by the average Nusselt and Sherwood numbers, which are defined respectively as

$$Nu = \int -(\partial\theta/\partial x)|_{x=0} \mathrm{d}y, \tag{5}$$

$$Sh = \int -(\partial c/\partial x)|_{y=0} \mathrm{d}x. \tag{6}$$

To describe the indoor air, heat and contaminant transport behaviours, visualization [1,18] of convective transport is presented.

According [19], the dimensionless stream-function (Ψ), heat-function (H) and mass-function (M), are defined as general function (F) which can be deduced from the conservative dimensionless transport equations of continuity, energy and concentration. For brevity, a compact definition according to the streamlines, masslines and heatlines was proposed using Eqs. (7) followed by the table:

$$\begin{cases} -\frac{\partial F}{\partial x} = v \cdot G - a_G \frac{\partial G}{\partial y} & (a) \\ \frac{\partial F}{\partial y} = u \cdot G - a_G \frac{\partial G}{\partial x}, & (b) \end{cases} \tag{7}$$

where the meanings of the dependent variable G, the diffusion coefficient a_G and the corresponding contour lines are listed as follows (u and v are the velocity components):

F	G	a_G	F contour plots
Stream-function (Ψ)	*1*	*0*	streamlines
Heat-function (H)	θ	$\frac{1}{Re\,Pr}$	*heatlines*
Mass-function (M)	c	$\frac{1}{Re\,Sc}$	*masslines*

3. Numerical procedure

Eqs. (2)–(4) are parabolic in time and elliptic in space. The temporal discretization of the time derivative is assumed by a second-order implicit scheme [20]. Non linear terms are evaluated explicitly; however, viscous terms are treated implicitly. The velocity–pressure coupling present in the continuity and the momentum equations is handled by using the projection method [21]. At each time step the scalar transport equations for energy and concentration are solved. Momentum equations for provisional velocity field are computed that may not be divergence free. A Poisson equation with homogeneous boundary conditions is then solved and leads to update pressure and free divergence velocity fields [22].

The spatial discretization of Eqs. (1)–(4) was made by the finite volume method [23–25] on a staggered grid system. It should be noted that the convective terms are discretized using the third-order accurate, quadratic upwind Quick scheme (Hayase et al. [26]).

All equations are solved using the red and black point successive over-relaxation (PSOR) method [27] with optimum relaxation factors, except the Poisson equation which is solved using an accelerated full multigrid method (FMG) [28,29] with the PSOR as smoother. Results provide the superiority of the FMG multigrid method against single grid calculations using the so-called V-cycle and optimal PSOR relaxation parameters. The global convergence was guaranteed by controlling the $L2$-residuals norm of all equations to be solved by setting its variation to less then 10^{-6}.

A non-uniform staggered grid was used in both directions; it is uniform and finer near the sources and uniform but coarser elsewhere. More precisely, we perform computations for both steady and time-dependent solutions with a grid of 96×96. The time steps Δt were varied between 10^{-2} and 2×10^{-3} depending on the values of the governing parameters of the study. Thus, for fixed values of Re, and at low or high values of Gr, the smallest values of Δt were used to ensure the convergence of numerical code. Mesh and time step sensitivity analysis revealed that with these values the solutions are accurate enough for our purposes.

4. Results and discussion

4.1. Steady state and code validation

There are some possibilities of validating the numerical code. One possibility is to compare the numerical results obtained by our code with benchmarks available in the literature according to different works. Another option is to simulate a similar problem investigated by other authors with well accepted available results. We believe that, the best validation may be performed against the work of Deng et al. [1]. As started in the introduction, the authors formulated the problem of the indoor air environment using a steady state model. Since the present model produces unsteady solution, the simulations were extended until reaching the steady regime in order to be able to compare with their results. As a matter of fact, we have reproduced all of their results but for convenience we have only chosen some of them for comparison. In order to prove that the streamlines, heatlines, and masslines provide a useful and simple means to visualize the flow, temperature, and contaminant concentration distributions, we first begin by comparing the solutions of the present work according to the Grashof number Gr effects in the steady laminar double-diffusive mixed convection in a two-dimensional ventilated enclosure as developed by Deng [1]. Fig. 2, shows the effects of the Grashof number Gr on the flow, temperature, and contaminant concentration distributions. The range of the Grashof number was varied in the range ($10^3 \leqslant Gr \leqslant 2.5 \times 10^4$) as shown in Fig. 2. The other parameters were kept constants: The Reynolds number $Re = 500$) and buoyancy ratio was assumed constant ($N = 1$). Flow topology, heat and mass distributions are fairly similar to those depicted by Deng et al. (see [1], Fig. 2 in page 5262, for comparison) in their paper.

Fig. 3a and b shows the comparison of the Nusselt and Sherwood values from the present model with the results due to Deng et al. [1] for $Re = 500$, $N = 1$ and for Gr in the range $10^3 \leqslant Gr \leqslant 2.5 \times 10^5$. It can be seen from these figures that both results are to in good agreement. The maximum difference between the two results is less then 2% and 2.5% for the heat and mass transfer rates, respectively.

At this stage, it may be concluded that our results agree quite well with those obtained by Deng et al. [1] and this validation shows that the present method only deals with steady laminar flows.

4.2. The unsteady flow investigation

4.2.1. Indoor airflow periodic mode at $Re = 700$

Most of the computations were carried out for a fixed value of the Reynolds number $Re = 700$ and at the monitoring point A (see Fig. 1). The Grashof number was varied in range $10^5 \leqslant Gr \leqslant 10^6$. To know the time-dependent behaviour of the flow, the variation of the x-component of velocity u with time has been considered and is depicted in Fig. 4, for different values of the Grashof number Gr and for $Re = 700$. We examined the transition of the flow by gradually increasing Gr. The question of when the flow becomes unsteady arises.

We found that the steady flow (Fig. 4a) corresponding to $Gr = 1.75 \times 10^5$ become unstable and was replaced by unsteady flow when Gr exceeds a threshold value. The periodic mode is displayed in Fig. 4b for $Gr = 2 \times 10^5$. Fig. 4c–j) shows that up to a Grashof number of 2×10^5 the two-dimensional flow in the indoor air environment remains periodic. Also, it is observed that the u-period values have a decreasing tend with increases in Gr. Obviously, all plots of Fig. 4 show a decrease in the u fluctuations magnitude. This can be attributed in fact that the main structure in the room is unchangeable except the periodic variation of small eddies near the heat and the contaminant sources.

Fig. 5 reports the variation of both frequency and period values corresponding to the periodic regime with Gr at $Re = 700$. As mentioned before, for Grashof number ranging approximately from 2×10^5 until 10^6, perfectly periodic solutions were obtained. Note that, this range of Gr is similar to that for the range (4.5×10^5–1.35×10^6) for which periodic solutions were obtained by May [30], in the case of free convection in a square enclosure with presence of sources. It can be seen from Fig. 5 that the frequency values increase monotonously without presenting any sign of change, i.e., the period of the oscillations decreases with increasing Gr.

Representative profiles at the monitoring point A of the room, for y-component velocity v, temperature θ and concentration c for various values of Grashof number and for $Re = 700$ were obtained but are not presented here. Taking for example, $Gr = 7 \times 10^5$ to illustrate and quantifying the time-dependent behaviour for all the fields studied, Fig. 6 shows that all fields are periodic with same period. The period τ of oscillation was found to be 6.579. The θ-amplitude in the critical mode ($Gr = 7 \times 10^5$) is, however, too small (Fig. 6b). The small values do not become strong in the range of Grashof number studied and thus play no active role in the change of the structures flow. However, the c-amplitude is particularly important as shown in Fig. 6c. Time evolution of the average Nusselt and Sherwood number produces similar oscillatory profiles with the same period value.

Examples of velocity and concentration spectrum at the monitoring point A are represented in Fig. 7. Both the

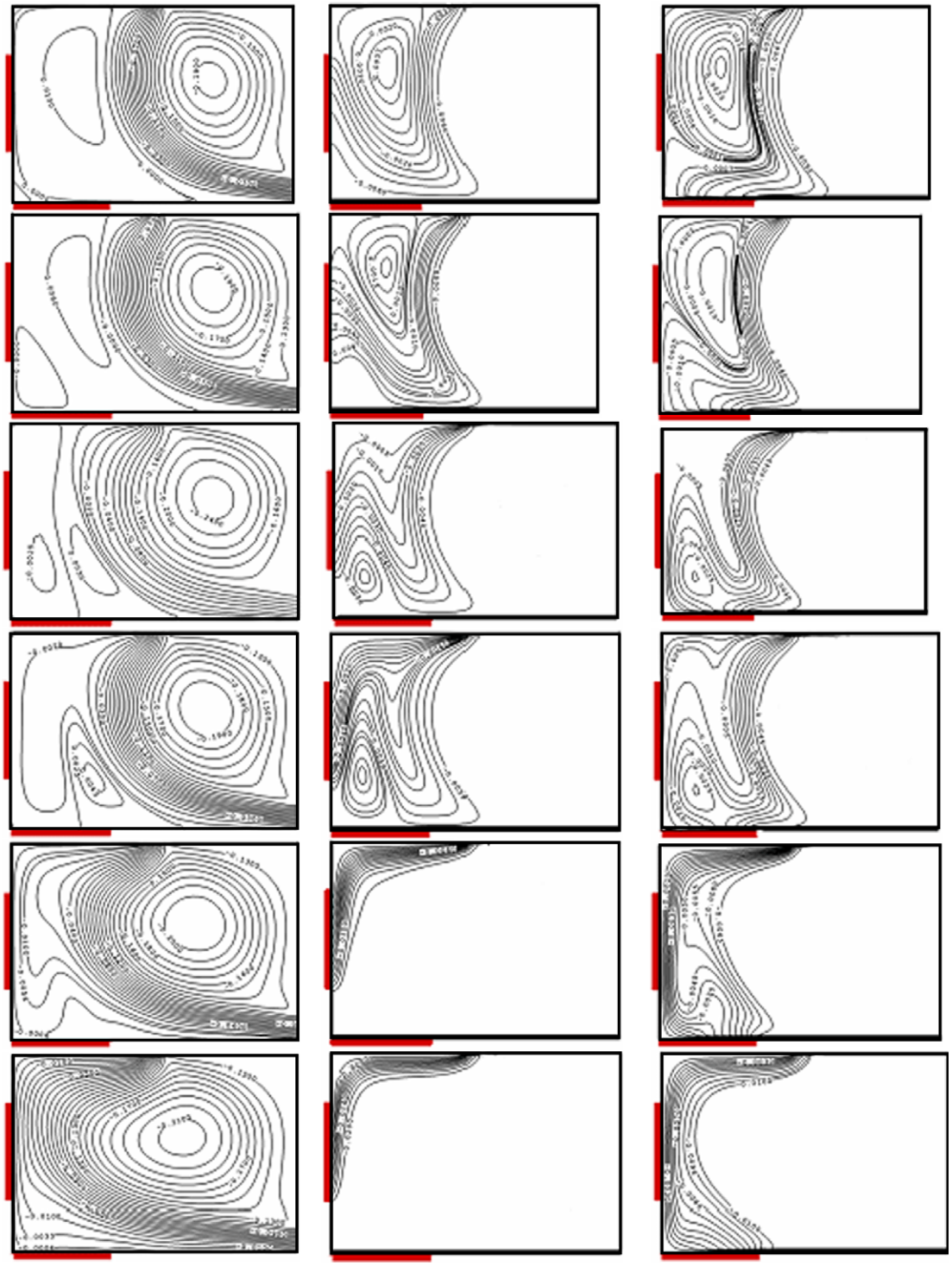

Fig. 2. Streamlines, heatlines and masslines from left to right for ($Re = 500, N = 1$) and ($Gr = 10^3, 10^4, 1.8 \times 10^4, 2.5 \times 10^4, 10^5, 2.5 \times 10^5$) from top to bottom.

figures exhibit markedly separate peaks corresponding to discrete frequencies, in accordance with the periodic nature of the flow. The highest peak occurs at the main period frequency ($f = 0.152$), while the secondary maxima correspond to its higher harmonics. The highest frequency still has significant amplitude approximatively equal to $2f$, for both, velocity and temperature.

To examine the heat transfer rate corresponding to the periodic regime, an average Nusselt number in time is defined as $Nu = [\max(Nu) + \min(Nu)]/2$, where $\max(Nu)$ and $\min(Nu)$ are the maximum and the minimum value of Nu, respectively. In the same way the average Sherwood number in time Sh is defined. This two parameters (Nu, Sh) are plotted at Reynolds number $Re = 700$ for various values

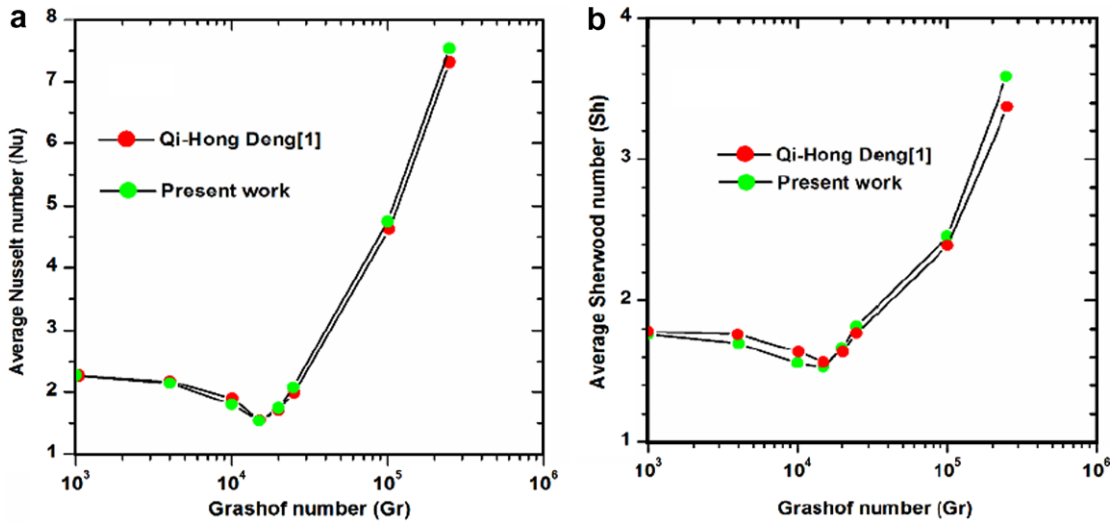

Fig. 3. Variation of average heat and mass transfer rates versus Gr number: comparison of present results with those of [1]: (a) average Nusselt number (b) average Sherwood number.

of Grashof number Gr in Fig. 8. Starting from the periodic state for $Gr = 5 \times 10^5$, Nu and Sh increase monotonously with Gr. In other words, heat and mass transfer are an increasing function with thermal buoyancy effect (Gr). The forced convection is strong enough but remains constant ($Re = 700$). Obviously, a positive buoyancy ratio ($N > 0$) leads to a situation of buoyancy aiding flow. Thus, the assisting buoyancy forces (thermal and solutal) act like a favourable pressure gradient which accelerates the heat and mass transfer of the fluid causing an increase of Nusselt (Nu) and Sherwood (Sh) numbers related to the periodic flow. For buoyancy opposing flow i.e. for negative values of (N) the situation will be certainly different. Further studies with large (N) ranges are necessary to clarify this point.

4.2.2. Effect of Re on the onset of the periodic mode

Several simulations have also been performed by varying the Reynolds number. Separate steady and periodic state are found at certain values of the two governing parameters Re and Gr. We only present the transition from steady to periodic regime by showing the time variation of the u-velocity at the monitor point A of the room. The results for three different values of Reynolds ($Re = 800$, 900 and 1000) are shown in Fig. 9.

The first simulation has been executed at $Re = 800$ starting from a steady solution corresponding to $Gr = 10^5$. The Grashof number Gr has been increased in steps of 0.25×10^5. At $Gr = 3 \times 10^5$ the flow is periodic with a period equal to 103.34 (Fig. 9a). The second simulation has been executed at $Re = 900$, starting from the solution obtained at $Gr = 10^5$: after a finite time interval $\approx$40 the flow becomes steady. A further increases in Gr at $Gr = 4.25 \times 10^5$ causes the transition to a periodic regime as shown in Fig. 9b (period equal to 143.45). The latest simulation has been executed at $Re = 1000$, starting from the solution obtained at $Gr = 10^5$. At $Gr = 5.75 \times 10^5$ the system undergoes a very long transient interval, before stabilizing on a periodic regime (Fig. 9c) with a highest period of 297.65. This situation corresponds to the limit of the stationary state.

4.2.3. Pattern periodicity at Re = 800

As mentioned above, the flow becomes periodic for $Re = 800$ and $Gr = 3 \times 10^5$. At this stage, we chose to present a short analysis of the periodicity associated with this Reynolds number. Thus, Fig. 10 shows the time histories of u, v, θ, and c profiles at the monitor point A. The periodic cycle reveals three interesting moments $T_0 = 63.54$, $T_1 = 107.90$ and $T_2 = 156.68$. These three different times are shown in Fig. 10 (and further in Fig. 11), correspond to the beginning (T_0), the intermediate (T_1), and almost the end of the period (T_2), respectively. It can be seen from Fig. 10 that the overall velocity magnitude obtained at the monitor point A is smaller than the magnitude corresponding to the concentration field with the temperature magnitude remaining weak. At $t = T_0$, various fields reach their minima. As time goes on, the concentration c increases when the v-velocity increases, but the u and θ curves seem to have the same flat region. In other words, the elevated v velocity component causes a substantial increase in the concentration profile, leading to more significant mass transfer of the contaminant. At time $t = T_2$ the concentration curve reaches a peak and drops sharply over a small time when u and v decrease indicating poorer entrainment. From the above description, we may thus conclude that the dimensionless time period (τ: $T_0 \rightarrow T_2$) includes two remarkable times T_0 and T_2: at the first one the removal contaminant process is slow; on the contrary, the removal contaminant efficiencies are more pronounced at the second. Moreover, the contaminant transfer is enhanced when the v velocity increases, until the next cycle.

In order to observe the characteristics of fluid and mass transport structures, the streamlines and masslines contours are plotted in Fig. 11 for $Re = 800$.

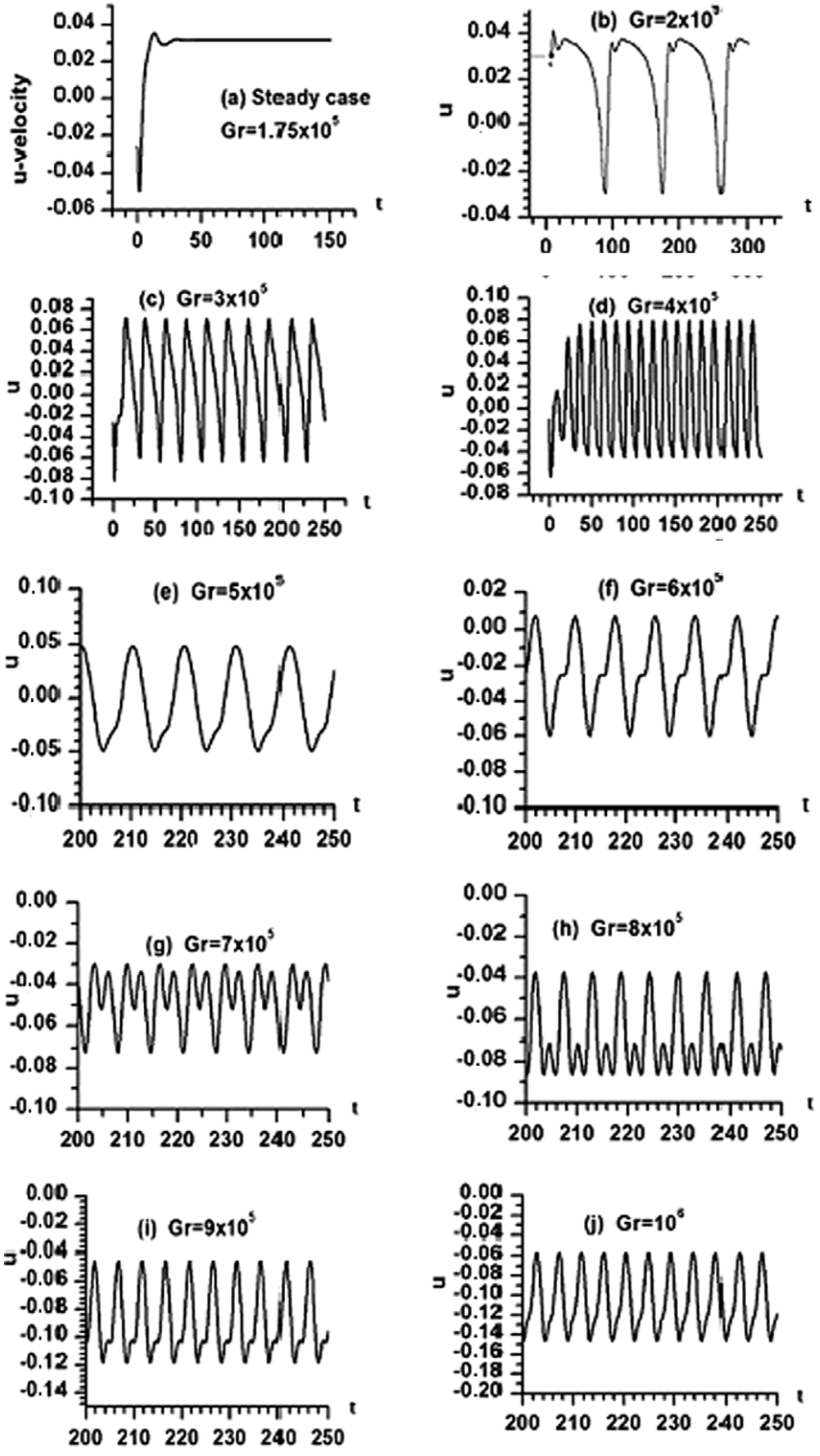

Fig. 4. Time evolution of the u-velocity at the monitoring point A (0.25, 0.125) for $Re = 700$ and at various Grashof numbers ($1.75 \times 10^5 \leqslant Gr \leqslant 10^6$).

Streamlines and masslines contours are first shown for the steady flow regime in Fig. 11a–b at $Gr = 2.75 \times 10^5$ and after, during a cycle of the period flow mode, which occurs at $Gr = 3 \times 10^5$, for three different instants namely T_0, T_1 and T_2 (cf. Fig. 10).

For the steady case, the airflow structure is shown in Fig. 11a in terms of streamlines. It consists of one large ventilated through-flow (negative ψ values) at the right part of the room, due to the forced convection, and two induced clockwise (negative ψ values) and counter-clockwise (posi-

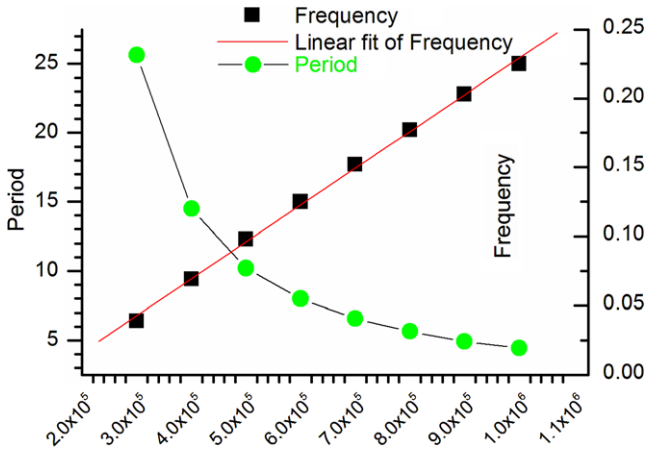

Fig. 5. Variation of the periodic state versus Gr at $Re = 700$.

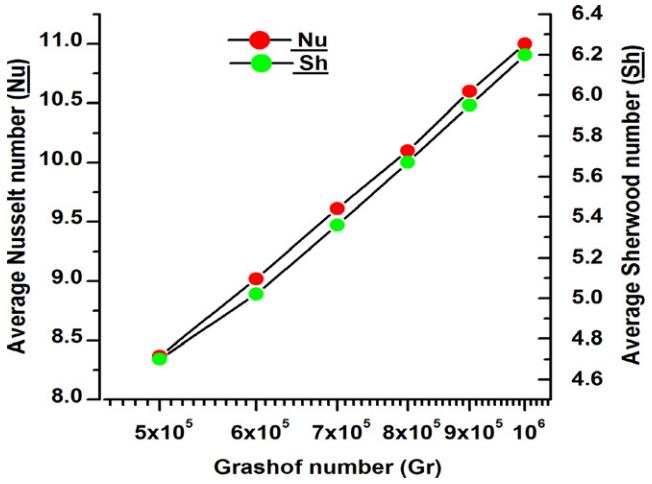

Fig. 8. Average Nusselt number and Sherwood number versus Gr at $Re = 700$.

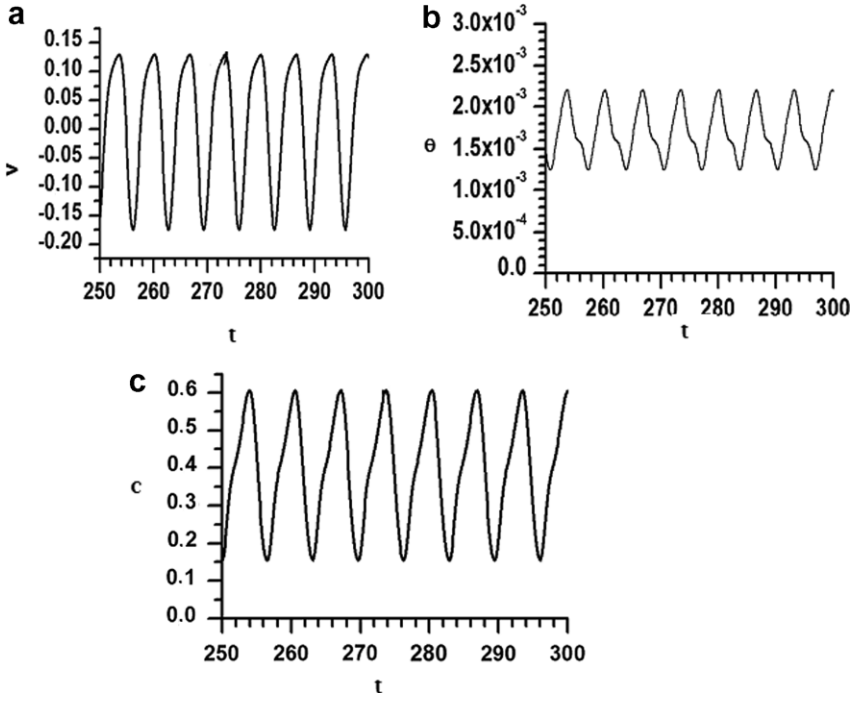

Fig. 6. Signal fields (v, c, θ) at the monitoring point A in the room for $Re = 700$ and $Gr = 7 \times 10^5$.

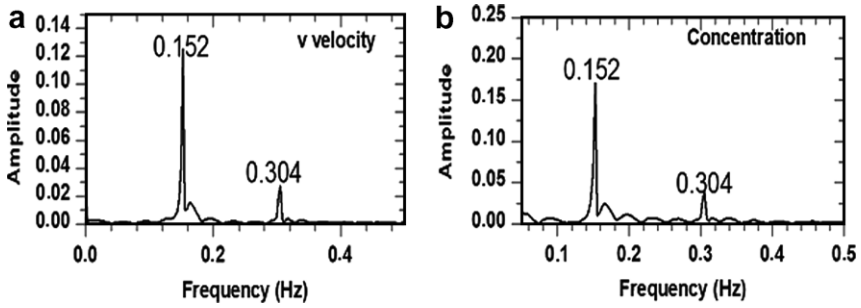

Fig. 7. Spectra of amplitude frequency for different fields, at the monitoring point A (0.25, 0.125) for $Re = 700$, $Gr = 7 \times 10^5$ and $N = 1$.

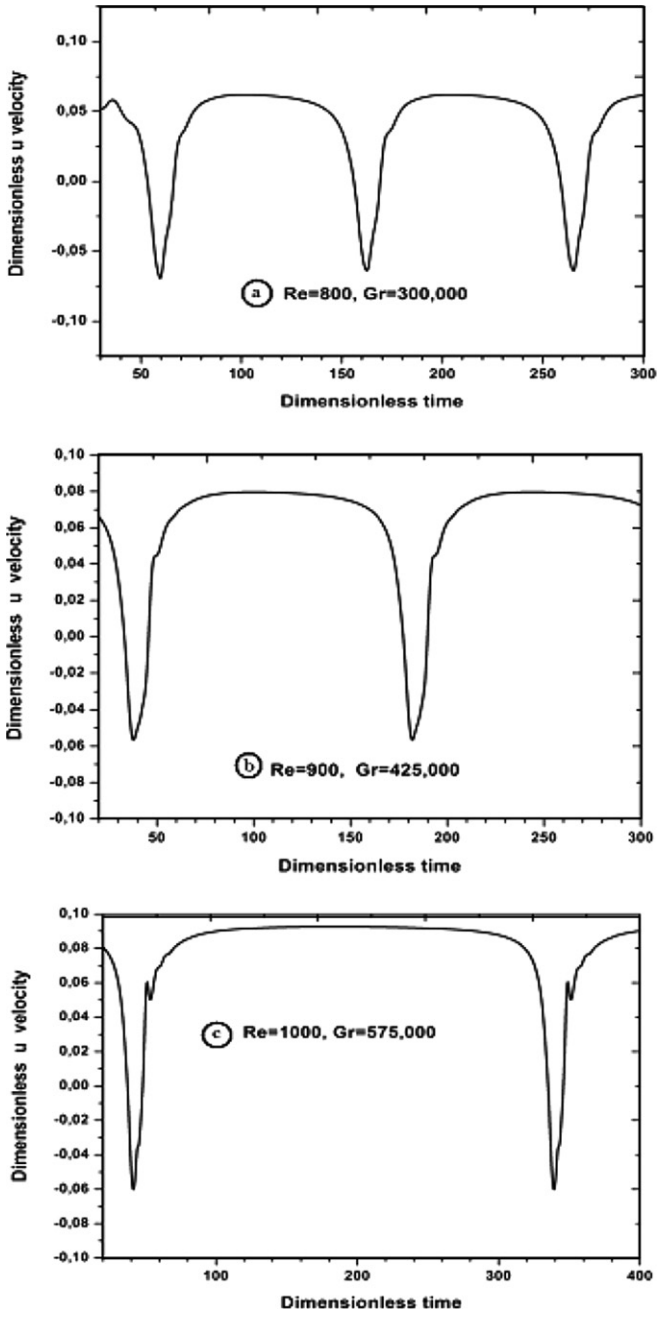

Fig. 9. u-Velocity signals at the monitoring point A (a–c), for $Re = 800$, 900 and 1000 respectively, and Gr just above the onset of instability.

tive ψ values) secondary circulating flows in the left parts of the room. One can observe that the masslines patterns are closely influenced by the airflow structure. Indeed, the ventilated airflow coming from inlet turns upward before it approaches the left wall, where it transports upward and carries out an important quantity of contaminant through the left sidewall. At this stage, on can say that most part of the contaminant is transported by ventilation (forced convection) and a big working area, as seen in Fig. 11b, being unaffected by the contaminant source. However, the masslines contour observed in the same figure, present a small counter-clockwise at the vicinity of the contaminant source which slows down the rise of the removal contaminant.

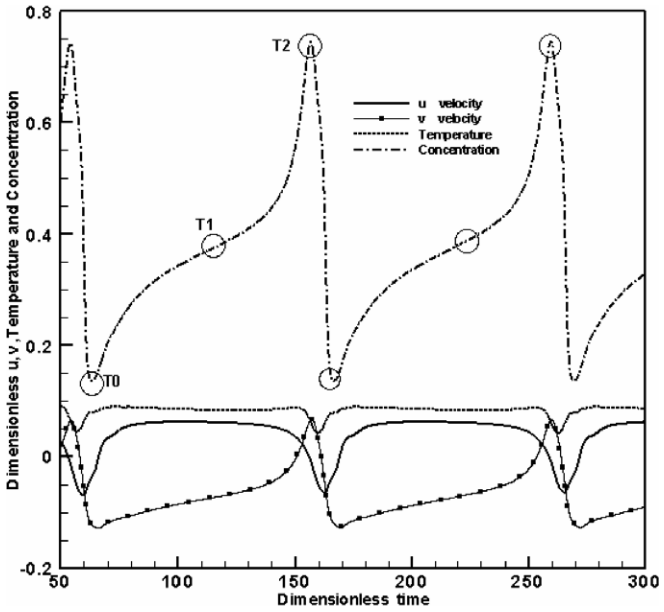

Fig. 10. Dimensionless u, v, θ and c time history at $Gr = 3 \times 10^5$ and $Re = 800$.

When the flow changes from steady to periodic regime, the airflow and masslines structures manifest some different behaviours comparing to the steady case during a period cycle. At $t = T_0$ of the chosen period (Fig. 11c), the counter-clockwise induced flow in the left part of the room, is slightly weakened. Consequently more contaminant escapes through the right side of this counter-clockwise. Certainly, the forced convection and the buoyancy forces were are enhanced enough, combine to disperse the contaminant. Therefore, the masslines would run through the entire room as observed in Fig. 11c. The working area that was useful in the steady case starts to disappear completely. In addition, we can observe the presence of a blocking contaminant area ($\psi = -0.0092$) as seen in Fig. 11d, from the contaminant source to the right sidewall leading to a dangerous aspect for health. This breaking contaminant sets in at $t = T_0$ and persists until $t = T_1$. At $t = T_1$, Fig. 11e shows that the secondary counter-clockwise induced flow is growing in size and thus slows down the contaminant removal process. However, the masslines patterns (Fig. 11f) at ($t = T_1$) are similar with those of the steady case ($t = T_0$). The reason for this shape is similar to those discussed in the context of Fig. 10. Subsequently, at the last phase of the periodic cycle ($t = T_2$) the large counter-clockwise induced flow, previously observed disappears and in place multiply counter-clockwise currents appear as observed in Fig. 11g. Consequently, the mass transfer is accelerated very sharply and diffuses in two directions: forwards and upwards (Fig. 11h). The blocking contaminant area starts to reproduce and will join the starting phase during the next period.

We consider that it is significant to minimize or to eliminate the danger zone while acting on certain flow parame-

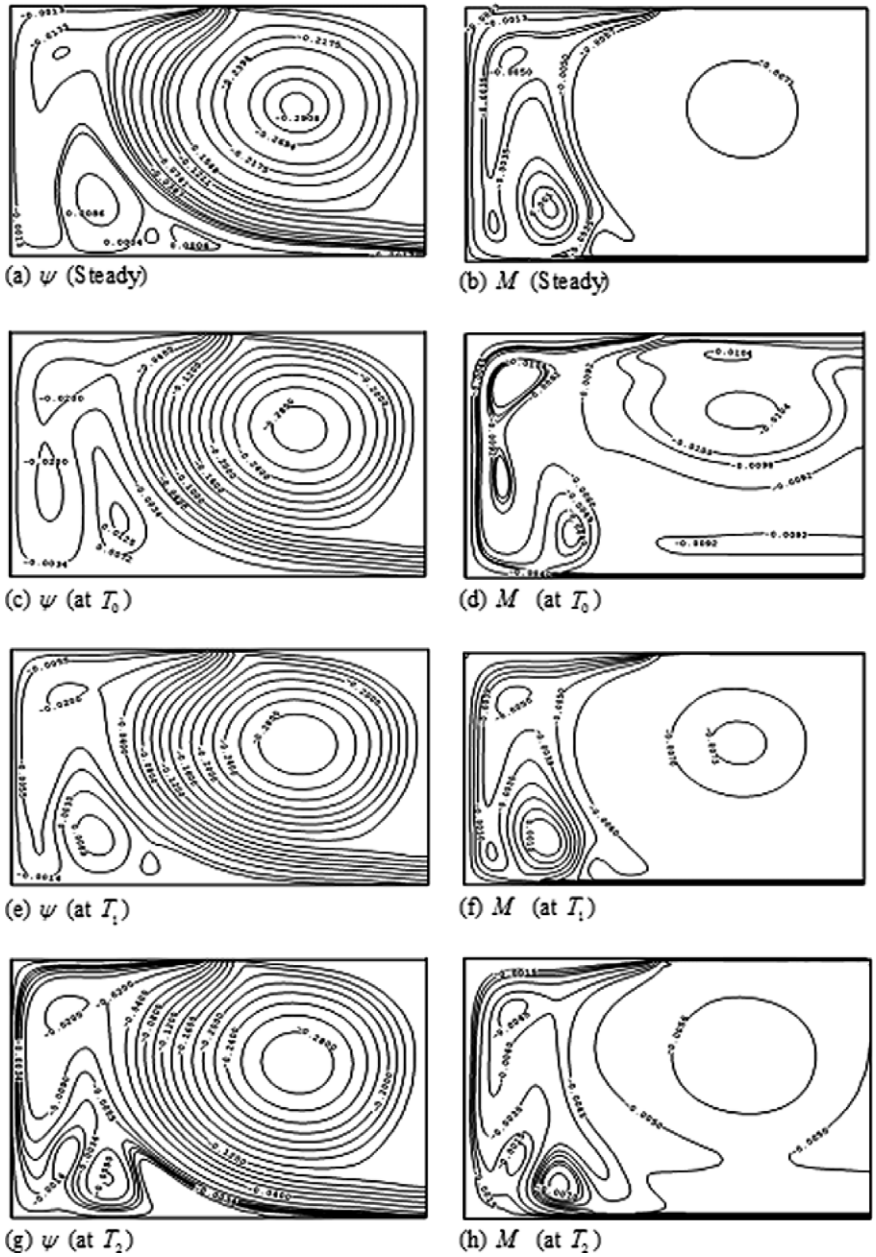

Fig. 11. Streamlines (ψ) and masslines (M) contours at $Re = 800$; steady case ($a - b$) at $Gr = 2.75 \times 10^5$, and periodic states (c–h) at $Gr = 3 \times 10^5$.

ters. We chose to vary the position of the outlet as well as its dimension. It is the object of the following paragraph.

4.2.4. Attempt to minimize the danger zone

With an aim of minimizing the danger zone that we have just highlighted previously ($Re = 800, Gr = 3 \times 10^5$), we chose to analyze the influence, on this blocking area, according to two geometrical parameters: the position as well as the width of the outlet located at the top side wall of the ventilated room.

4.2.4.1. Effect of the width. We tested several values of the width of the outlet, always occupying the centre of the top wall, namely h, 2h, 4h, 6h and 8h. (h being the dimensional width of the inlet room).

For all these values the flow remains periodic and the results of simulation show that the period of the flow decrease in an appreciable way when the outlet width increases as seen in Fig. 12a. In parallel, the heat and mass transfer decrease slightly compared to the reference case as shown in Fig. 12b.

The examination of the masslines shapes relating to these various values of the outlet width confirmed the persistence of the blocking area. At this stage, we can conclude that the parameter relating to the variation of the outlet width is not able to eliminate the dangerous zone.

4.2.4.2. Effect of the position. We tested several outlet positions of X-coordinates $X/h = 0.125, 0.25, 0.5, 0.75$, and 1.0, as shown in Fig. 13a. This figure represents the variations

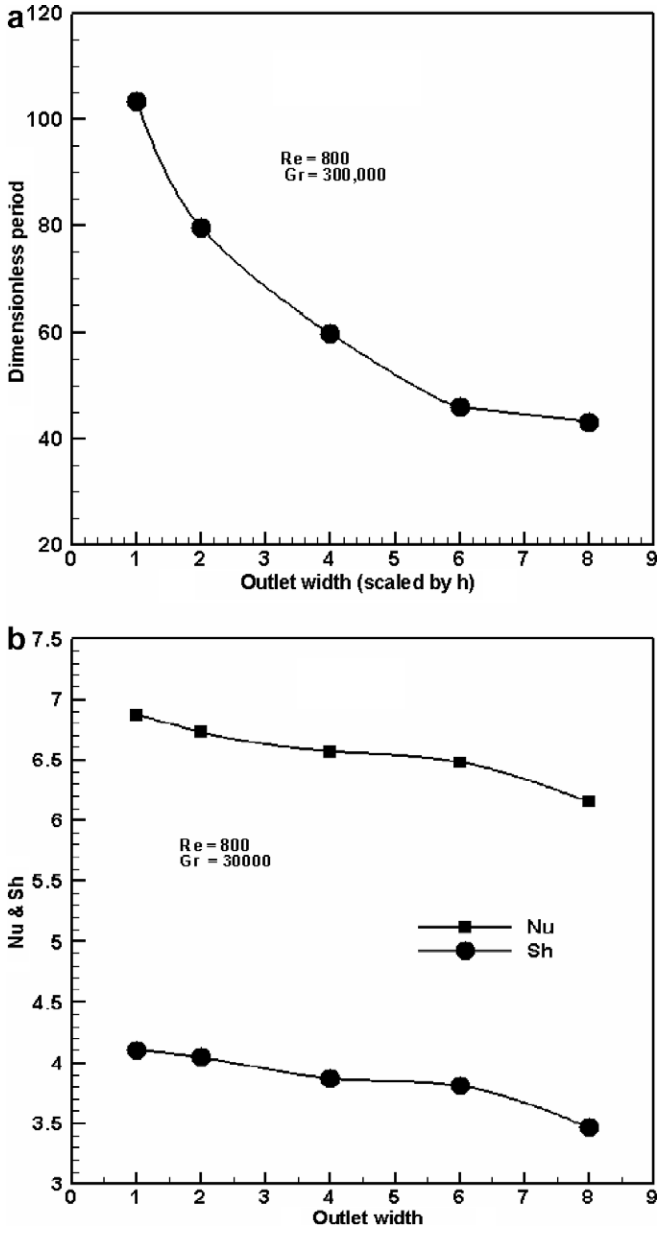

Fig. 12. Periodic values versus outlet width (h, $2h$, $4h$, 6h and $8h$).

of Nusselt (Nu) and Sherwood (Sh) numbers for these various positions.

Let us specify the disappearance of the periodic flow mode and the establishment of a stationary state for the cases represented by the X-coordinates $X/h = 0.125$ and 0.25. As clearly for the positions $X/h = 0.5$, 0.75 and 1, the flow remains periodic.

The examination of the masslines shapes relating to these various positions shows obviousness that the optimal position leading to the elimination of the danger zone corresponds to the position $X/h = 0.125$ as shown in Fig. 13b.

4.2.5. Influence of the periodic regime on heat and mass transfer rates

Fig. 14 plots the variation of both average Nusselt and Sherwood numbers corresponding to the steady case,

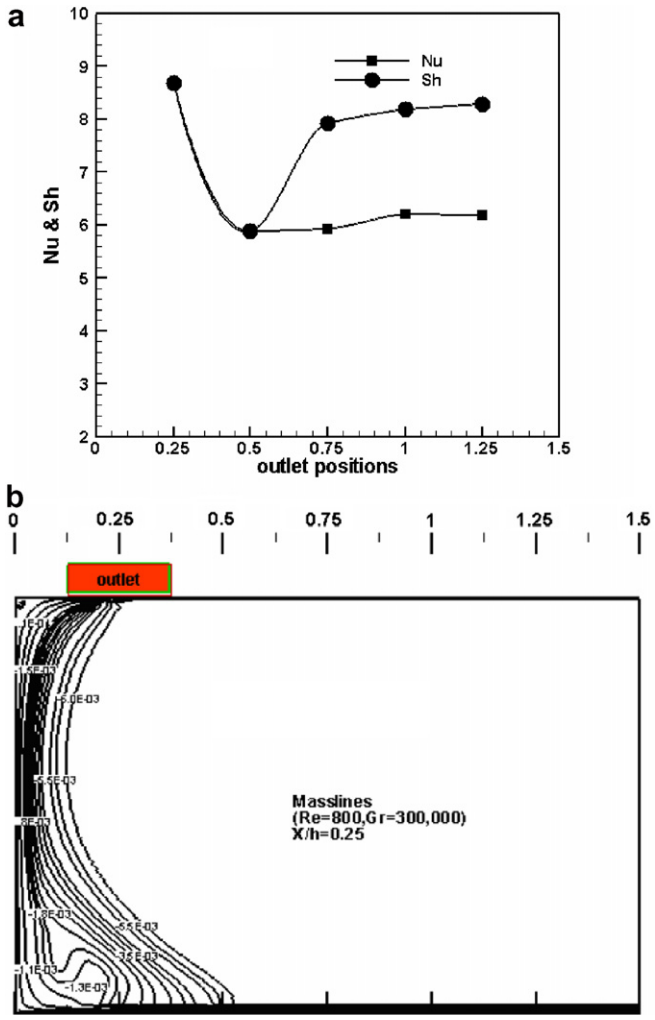

Fig. 13. (a) Outlet positions, (b) masslines contour ($Re = 800$, $Gr = 300{,}000$) at the location $X/h = 0.25$.

namely Nu and Sh, and to the periodic state namely Nu and Sh, in terms of the governing parameter Gr/Re^2. The average Nusselt number for periodic flow is shown to be higher than the steady flow. This is because more buoyancy strength is needed to obtain periodic flow for a higher Gr than that for a lower Gr. Precisely, in the range ($0.4 \leqslant Gr/Re^2 \leqslant 0.55$) the mean heat transfer rate obtained from the periodic state is about 10% higher than that of the steady case.

In addition, as shown in Fig. 14, the unsteady Sherwood number (Sh) increases with respect to the $\frac{Gr^2}{Re}$ parameter. The raison for this is that an increase in the strength of the external forced flow (ventilation) leads to an acceleration of the room airflow, which increases the mass transfer rate. The results reveal that both steady and periodic Sherwood numbers (Sh) and (Sh); respectively, seems to have the same trend.

In order to detect when the release of the periodic mode is carried out, the couples (Gr, Re) for which the regime of flow becomes periodic for the first time are presented in Fig. 15. The onset of the oscillatory behaviour of the flow is depicted

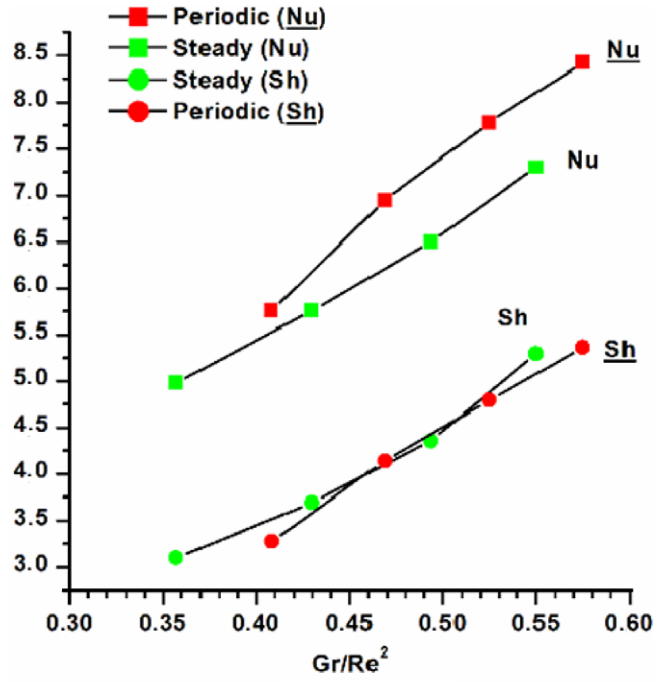

Fig. 14. Average Nusselt and Sherwood Numbers (periodic and steady cases) versus Gr/Re^2.

with a maximum errors bar of 2.5×10^5 in the Grashof number Gr. It can be deduced from this figure that the higher the Reynolds number Re, the larger the Grashof number required to reaching the first periodic state of the flow.

Based on numerical results, a correlation of the Reynolds number, Re versus the Grashof number, Gr is obtained by using a linear fit of the periodic regime and expressed as:

$$Re = 11.285 Gr^{0.338} \tag{8}$$

for the range of experiments performed here (ranges of validity: $700 \leqslant Re \leqslant 1000$ and $2 \times 10^5 \leqslant Gr \leqslant 6 \times 10^5$). The numerical values and the proposed correlation (Eq. (8)) are seen to agree with a maximum deviation of 0.2%.

The graph indicates that the region above the correlation curve corresponds to the steady regime in the ventilated room. Fourth more, the oscillations enter a more irregular state beyond the correlation curve, eventually turning into aperiodic mode, but the exact evolution from this point (i.e. the right region) is outside the scope of this work. Note that the simplified model (Eq. (8)) could be of some interest in the indoor air environment involving unsteadiness in double-diffusive mixed convection phenomenon. This allows concluding that the indoor air regime is mainly controlled by both forced convection (Re), buoyancy thermal (Gr) and mass driven forces.

5. Conclusion

Unsteady heat and mass transfer by double-diffusive mixed convection in two-dimensional ventilated room was studied numerically. Based on the result and analysis

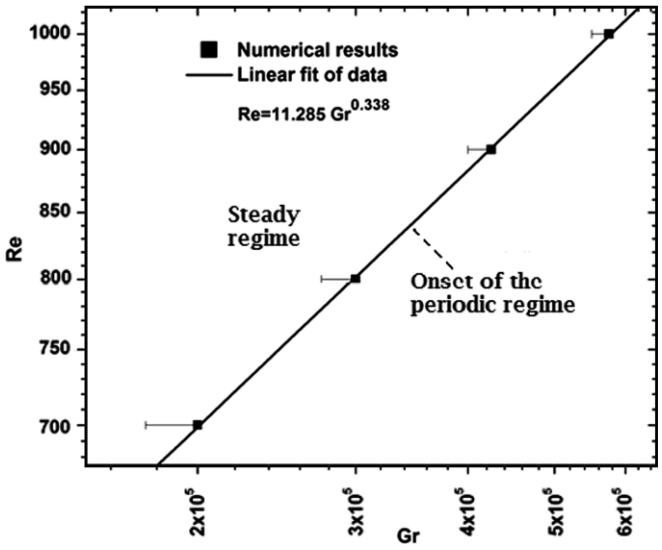

Fig. 15. Correlation curve (Re as function of Gr).

of the numerical experiment the following conclusion is made:

1. The steady state result was found close to those obtained by Deng et al., and the validation showed the ability of the present method to deal with transient double-diffusive problems.
2. For $Re = 700$, the critical value of Grashof number relative to transition from steady to periodic flow was found to be at $Gr = 2 \times 10^5$. Up to this value, the flow remains periodic. The period of oscillations decreases whereas the main heat and transfer rates increase monotonously with increasing Gr.
3. Representative profiles at a fixed point of the enclosure showed that all fields were periodic with the same period at $Re = 700$ as revealed for a particular Grashof number $Gr = 7 \times 10^5$. A similar behaviour was observed in terms of average Nusselt and Sherwood numbers.
4. With the practical visualizations using streamlines, heatlines, and masslines, it was observed at $Re = 800$ that the periodic cycle contains slow and active moments for the removal contaminant efficiencies. A blocking contaminant area appearing the cycle leads to a dangerous aspect for health. An attempt to minimize the contaminated danger zone reveals that the optimal outlet position is located at the left top wall of the room.
5. The main heat rate obtained at the onset of the periodic regime is about 10% higher than that of the steady case when the ratio Gr/Re^2 is in range (0.4–0.5) whereas the mass transfer rate remains unchanged by periodic behaviour.
6. For different Reynolds numbers considered in this study, the Grashof numbers leading to the onset of oscillations can be correlated by the relationship: $Re = 11.285 Gr^{0.338}$.

7. The average Nusselt number for periodic flow is shown to be higher than that of steady case. This is because more oscillatory flow attained at a higher Gr.

Future work will include extensions to the buoyancy ratio the effects and analysis of stability and bifurcations.

Acknowledgments

We would like to express our sincere thanks to the referees for the constructive suggestions and useful comments to improve this paper.

References

[1] Qi-Hong Deng, Jiemin Zhou, Chi Mei, Yong-Ming Shen, Fluid, heat and contaminant transport structures of laminar double-diffusive mixed convection in a two-dimensional ventilated enclosure, Int. J. Heat Mass Transfer 47 (2004) 5257–5269.
[2] C. Béghein, F. Haghighat, F. Allard, Numerical study of double-diffusive natural convection in a square cavity, Int. J. Heat Mass Transfer 35 (4) (1992) 833–846.
[3] J. Tanny, B. Yakubov, Experimental study of a double-diffusive two-layer system in a laterally heated enclosure, Int. J. Heat Mass Transfer 42 (1999) 3619–3629.
[4] M. Mamou, P. Vasseur, M. Hasnaoui, On numerical stability analysis of double-diffusive convection in confined enclosures, J. Fluid Mech. 433 (2001) 209–250.
[5] Ruixian Cai, Chenhua Gou, Exact solutions of double diffusive convection in cylindrical coordinates with $Le = 1$, Int. J. Heat Mass Transfer 49 (2006) 3997–4002.
[6] K. Shi, W. Lu, The evolution of double diffusive convection in a vertical cylinder with radial temperature and axial solutal gradients, Int. J. Heat Mass Transfer 49 (2006) 995–1003.
[7] A.P. Jones, Indoor air pollution and health, Atmos. Environ. 33 (1999) 4535–4564.
[8] K.C. Chung, Three-dimensional analysis of airflow and contaminant particle transport in a partitioned enclosure, Build. Environ. 34 (1999) 7–17.
[9] Q.-H. Deng, G.-F. Tang, Numerical visualization of mass and heat transport for conjugate natural convection/heat conduction by streamline and heatline, Int. J. Heat Mass Transfer 45 (11) (2002) 2373–2385.
[10] Qi-Hong Deng, Guoqiang Zhang, Indoor air environment: more structures to see? Build. Environ. 39 (2004) 1417–1425.
[11] K. Gorayeb, H. Khallouf, A. Mojtabi, Onset of oscillatory flows in double-diffusive convection, Int. J. Heat Mass Transfer 42 (4) (1999) 629–643.
[12] I. Sezai, A.A. Mohamad, Double diffusive convection in a cubic enclosure with opposing temperature and concentration gradients, Phys. Fluids 12 (9) (2000) 2210–2223.
[13] S. Roy, Anil kumar, Unsteady mixed convection from a rotating cone in a rotating fluid due to the combined effect of thermal and mass diffusion, Int. J. Heat Mass Transfer 45 (4) (2002) 1345–1352.
[14] T. Nishimura, M. Wakamatsu, A.M. Morega, Oscillatory double-diffusive convection in a rectangular enclosure with combined horizontal temperature and concentration gradients, Int. J. Heat Mass Transfer 41 (11) (1998) 1601–1611.
[15] A. Mahidjiba, M. Mamou, P. Vasseur, Onset of double-diffusive convection in a rectangular porous cavity subject to mixed boundary conditions, Int. J. Heat Mass Transfer 43 (2000) 1505–1522.
[16] J.M. Zhan, Y.S. Li, Numerical simulation of unsteady flow in natural and thermosolutal convection using boundary-fitted coordinate system, Int. J. Numer. Method. H 13 (8) (2003) 1031–1056.
[17] Kefeng Shi, Wen-Qiang Lu, Evolution of double-diffusive convection in a vertical cylinder with radial temperature and axial solutal gradients, Int. J. Heat Mass Transfer 49 (2006) 995–1003.
[18] Al.M. Morega, A. Bejan, Heatline visualization of forced convection boundary layers, Int. J. Heat Mass Transfer 36 (1993) 3957–3966.
[19] V.A.F. Costa, Unification of the streamline, heatline and massline methods for the visualization of two-dimensional transport phenomena, Int. J. Heat Mass Transfer 42 (1) (1999) 27–33.
[20] D. Kim, H. Choi, A second-order time-accurate finite volume method for unsteady incompressible flow on hybrid unstructured grids, J. Comput. Phys. 162 (2000) 411–428.
[21] D.L. Brown, R. Cortez, M.L. Minion, Accurate projection methods for the incompressible Navier-Stokes equations, J. Comput. Phys. 168 (2001) 464–499.
[22] S. Abide, S. Viazzo, A 2D compact fourth-order projection decomposition method, J. Comput. Phys. 206 (2005) 252–276.
[23] S.V. Patankar, A calculation procedure for two-dimensional elliptic situations, Numer. Heat Transfer 34 (1981) 409–425.
[24] F. Moukhalled, M. Darwish, A unified formulation of the segregated class of algorithm for fluid flow at all speeds, Numer. Heat Transfer B 37 (2000) 103–139.
[25] M.H. Kobayachi, J.M.C. Pereira, J.C.F. Pereira, A conservative finite-volume second-order-accurate projection method on hybrid unstructured grids, J. Comput. Phys. 150 (1999).
[26] T. Hayase, J.A.C. Humphrey, R. Greif, A consistently formulated QUICK scheme for fast and stable convergence using finite-volume iterative calculation procedures, J. Comput. Phys. 98 (1992) 108–118.
[27] William H. Press, Numerical recipes in Fortran 77: the art of scientific computing, vol. 1, second ed., 1997.
[28] Y. Jiang, C.P. Chen, P.K. Tucker, Multigrid solutions of unsteady Navier-Stokes equations using a pressure method, Numer. Heat Transfer—Part A 20 (1991) 81–93.
[29] M.S. Mesquita, M.J.S. de Lemos, Optimal multigrid solutions of two-dimensional convection-conduction problems, Appl. Math. Comput. 152 (2004) 725–742.
[30] H.O. May, A numerical study on natural convection in an inclined square enclosure containing internal heat sources, Int. J. Heat Mass Transfer 34 (1991) 919–928.